Supporting Information

Effective hydrogen isotope separation by a robust flexible calix[4]resorcinarene-based porous organic cage

Yanan Guo,[a,b] Jiajun Feng,[a,b] Wenjing Wang,[b,c] Kongzhao Su*[b,c] and Daqiang Yuan*[b,c]

[a] College of Chemistry, Fuzhou University, Fuzhou, 350116, People's Republic of China

[b] State Key Lab of Structure Chemistry, Fujian Institute of Research on the Structure of Matter, Chinese Academy of Sciences, Fuzhou, 350002, People's Republic of China

[c] University of the Chinese Academy of Sciences, Beijing, 100049, People's Republic of China.

E-mail: skz@fjirsm.ac.cn; ydq@fjirsm.ac.cn

Section S1. General Materials and Measurements

All the reagents were purchased from the market and no further purification was necessary, while the ligand CR4ACHO (tetraformylcalix[4]resorcinarene) was synthesized using the method described in the literature procedure.[S1] ^{1}H NMR spectra were recorded on a Bruker Avance 400 spectrometer operating at 400 MHz. Fourier transform infrared (FT-IR) spectra were recorded on a Vertex 750 spectrometer using the KBr pellet method, covering a wavenumber range from 4000 to 500 cm^{-1}. TGA measurements were carried out on a STA 449F3 analyzer with approximately 5-10 mg of sample in an alumina crucible, under a nitrogen atmosphere, at a heating rate of 10 °C/min from room temperature to 800 °C. The morphology was observed with a SU8010 scanning electron microscope (SEM). MALDI-TOF mass spectra were acquired on a Bruker ultrafleXtreme spectrometer. Powder X-ray diffraction (PXRD) patterns were recorded on a Rigaku Mini 600 diffractometer using Cu Kα radiation (λ = 1.54 Å). PXRD simulations were conducted utilizing the Mercury software package (employing the single crystal data and diffraction crystal module), which is available free of charge at http://www.ccdc.cam.ac.uk/products/mercury/.

Adsorption/desorption experiments

The N_2, H_2 and D_2 adsorption-desorption isotherms of the adsorbent were measured using a BSD Series 660M-0162 (High-Performance) Gas Sorption Analyzer at 77 K and 87 K, respectively. Prior to gas adsorption measurements, CPOC-F301, CPOC-301, and SMS-POC-1 were subjected to solvent exchange every 24 hours over a five-day period. Approximately 100 mg of the solvent-exchanged samples was thermally activated at 373 K for 12 h. Nitrogen (N_2) physisorption isotherms were acquired at 77 K using a Micromeritics ASAP 2020 Plus surface area and porosity analyzer. Temperature control during H_2/D_2 adsorption was achieved using liquid nitrogen (for 77 K) and liquid argon (for 87 K) as cooling media. Pore size distribution analysis was derived from the N_2 adsorption isotherm at liquid nitrogen temperature by applying the DFT model (cylindrical pore geometry assumed) embedded in the Micromeritics ASAP 2020 software. The material underwent an activation

pretreatment by being degassed at 373 K for 12 hours before the gas adsorption measurements, ensuring a clean surface for accurate analysis.

Breakthrough Measurements

Dynamic gas breakthrough experiments were performed using a BSD-MAB dynamic gas breakthrough system. Specifically, three samples (CPOC-F301, CPOC-301, and SMS-POC-1) were individually packed into 1 mL quartz column, with a small amount of quartz wool filled at both ends of each column to secure the samples. Prior to breakthrough testing, the samples were activated at 373 K for 12 h under a continuous neon (Ne) flow of 8 mL/min. The breakthrough column was left in a cooling medium-filled Dewar flask for ~20 min to equilibrate, followed by the breakthrough test. Dynamic breakthrough experiments were conducted using a H_2/D_2/Ne (3/3/94, vol%) gas mixture at a flow rate of 8 mL/min, with the flow rate controlled by a precision mass flow controller. The sample was regenerated by purging with neon gas at a flow rate of 8 mL/min at 100 °C for 120 min, in preparation for the cycling tests.

The complete breakthrough of D_2 was identified when the composition of the downstream effluent matched that of the feed gas. The adsorption capacity was then calculated based on a mass balance, as given by the following equation.

$$q_i = \frac{C_i V}{22.4} \times \int_0^t \left(1 - \frac{F}{F_0}\right) dt \quad \textbf{(Equation 1)}$$

Where q_i refers to the equilibrium adsorption capacity of gas i (mmol·g^{-1}), C_i representsthe feed gas concentration, V refers to the volumetric feed flow rate (cm^3·min^{-1}), t represents the adsorption time (min), F and F_0, respectively, refer to the inlet and outlet gas molar flow rates, and m represents adsorbent mass of (g). The separation factor (α) of breakthrough experiment can be calculated as follows:

$$\alpha = \frac{q_A y_B}{q_B y_A} \quad \textbf{(Equation 2)}$$

In which y_i is molar fraction of gas i (i=A, B) in gas mixture.

Isosteric heat of adsorption calculations

The data were fitted using a virial-type model incorporating parameters a_i and b_j (**Equation 3**). The isosteric heat of adsorption (Qst) was determined from the fitting parameters according to **Equation 4**, which was derived from the D_2/H_2 adsorption isotherms.

$$\ln(P) = \ln(N) + \frac{1}{T}\sum_{i=0}^{m} a_i N^i + \sum_{j=0}^{n} b_j N^j \quad \textbf{(Equation 3)}$$

$$Q_{st} = -R\sum_{i=0}^{m} a_i N^i \quad \textbf{(Equation 4)}$$

IAST calculations of adsorption selectivity

To evaluate the separation capability of the material for D_2/H_2, pure-component isotherms were fitted using the single-site Langmuir-Freundlich equation, and the molar loadings in the mixture under specified bulk gas-phase partial pressures were determined (**Equation 5**). The adsorption selectivity for D_2/H_2 mixtures, based on the Ideal Adsorbed Solution Theory (IAST), was calculated using **Equation 6**.

$$N = A_1\frac{b_1 P^{c1}}{1 + b_1 P^{c1}} \quad \textbf{(Equation 5)}$$

$$S_{A/B} = \frac{x_A y_B}{x_B y_A} \quad \textbf{(Equation 6)}$$

Section S2. Single-Crystal X-ray Crystallography

Single-Crystal X-ray Crystallography: Single-crystal X-ray diffraction data for **CPOC-F301** were collected on an XtaLAB Synergy R, HyPix diffractometer equipped with a PhotonJet R (Cu) X-ray source (λ = 1.5406 Å). The crystal structure was solved by direct methods and refined using the SHELXTL-2018 program package.[S2] All non-hydrogen atoms were refined anisotropically. Hydrogen atoms of the organic ligands were placed in calculated positions using a riding model and refined with isotropic displacement parameters. The crystal structure was further processed using the SQUEEZE routine implemented in the PLATON software package to account for disordered solvent molecules.[S3, 4] Detailed crystallographic data and cell parameters for **CPOC-F301** are summarized in Table S1.

Table S1. Crystallographic Data and Structure Refinement for **CPOC-F301.**

	CPOC-F301
Formula	$C_{360}H_{452}N_{24}O_{48}$
M / g mol^{-1}	5883.48
T / K	100
Crystal system	tetragonal
Space group	*P*4/n
***a* / Å**	32.1810(5)
***b* / Å**	32.1810(5)
***c* / Å**	37.8481(12)
***α* (°)**	90
***β* (°)**	90
***γ* (°)**	90
V / Å^3	39196.1(17)
Z	2
***μ* (mm^{-1})**	0.262
Data measured	99048
Ind. reflns	34253
Parameters	946
GOF on F^2	0.962
R_1[a] [I ›σ(I)]	0.0902
wR_2[b]	0.2777
CCDC number	2498812

[a]$R_1 = \sum||F_o| - |F_c||/\sum|F_o|$. [b]$wR_2 = \{\sum[w(F_o^2 - F_c^2)^2]/\sum[w(F_o^2)^2]\}^{1/2}$

Section S3. Synthetic Procedures and Characterizations

Synthesis of **CPOC-F301**:

C4RACHO (0.1 mmol, 41 mg) and trans-1,4-cyclohexanediamine (0.2 mmol, 12 mg) were dissolved in 6 mL of $CHCl_3$ in a 20 mL pressure-resistant vial. The mixture was sealed and stirred overnight at 65 °C. After cooling to room temperature, the solution was equally distributed into 20 mL glass vials. Subsequently, 0.5 mL of $PhNO_2$ was added to each vial, and red block-shaped crystals of **CPOC-F301** were obtained by slow vapor diffusion of methanol over one week. The crystals were washed with methanol, yielding 69%. ^{1}H NMR (400 MHz, CDCl3, 298 K): δ 14.60 (s, 1H), 11.19 (s, 1H), 8.66 (s, 1H), 7.24 (s, 1H), 4.53 (t, 1H), 2.07 (d, 1H), 1.96–1.89 (m, 1H), 1.52 (dd, 1H), 1.25 (s, 1H), 0.98(t, 6H) p.p.m. MALDI-TOF-MS: $[M+NH_4]^+$ calcd. for CPOC-F301 ($C_{360}H_{456}N_{25}O_{48}$) is 5901.624; found 5901.310.

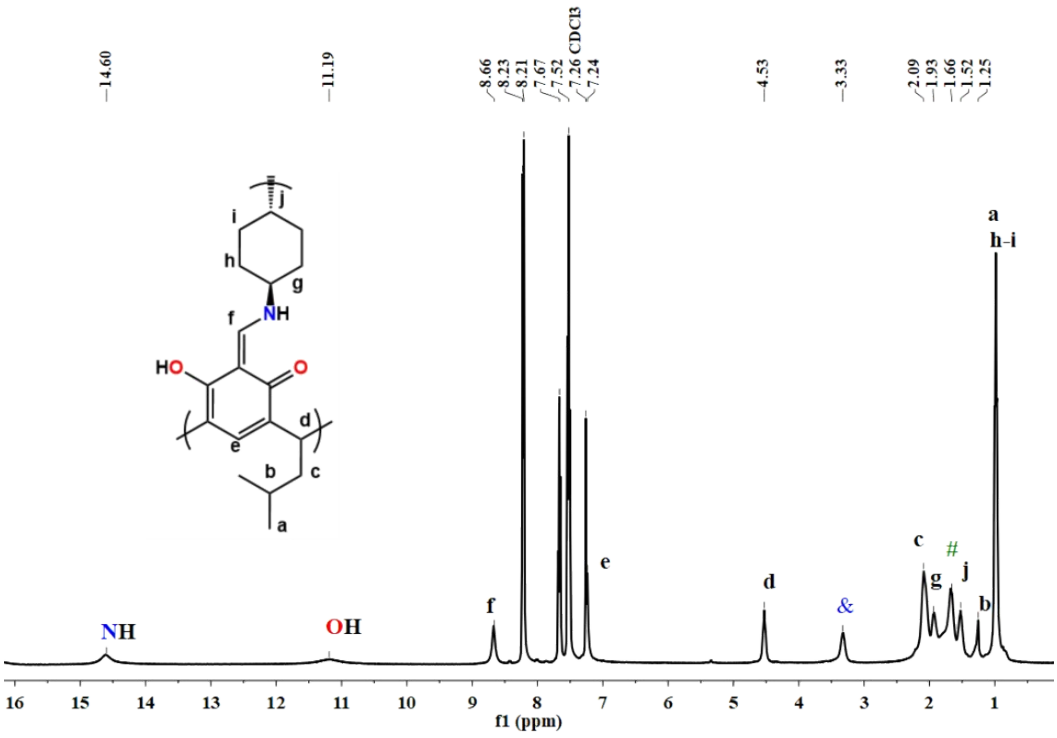

Figure S1. ^{1}H NMR spectrum of **CPOC-F301**. (The marked extra peaks, $^{\&}CH_3OH$, $^{\#}H_2O$. The signals in the 7-9 ppm range are assigned to nitrobenzene.)

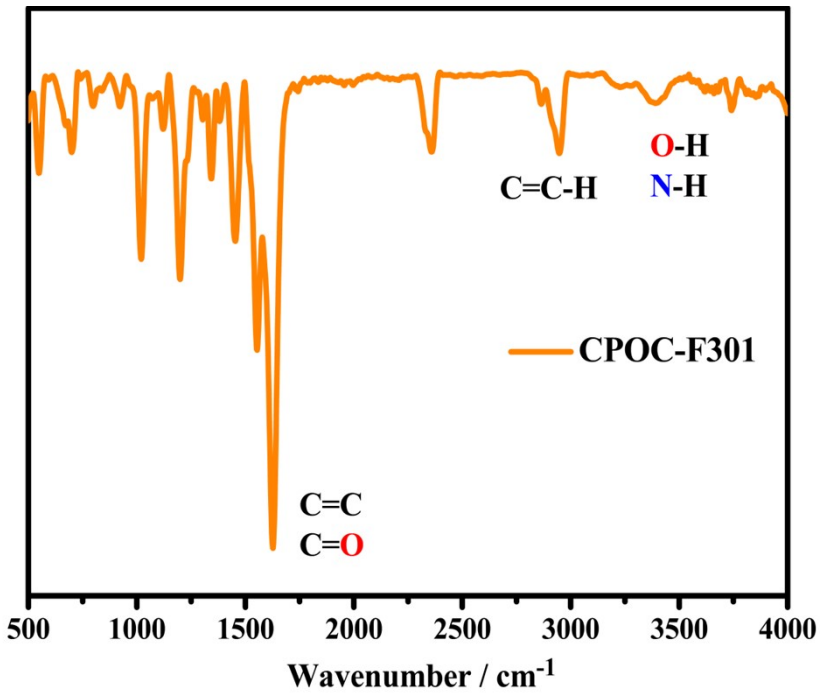

153

154 **Figure S2.** FT-IR spectrum of **CPOC-F301.**

155

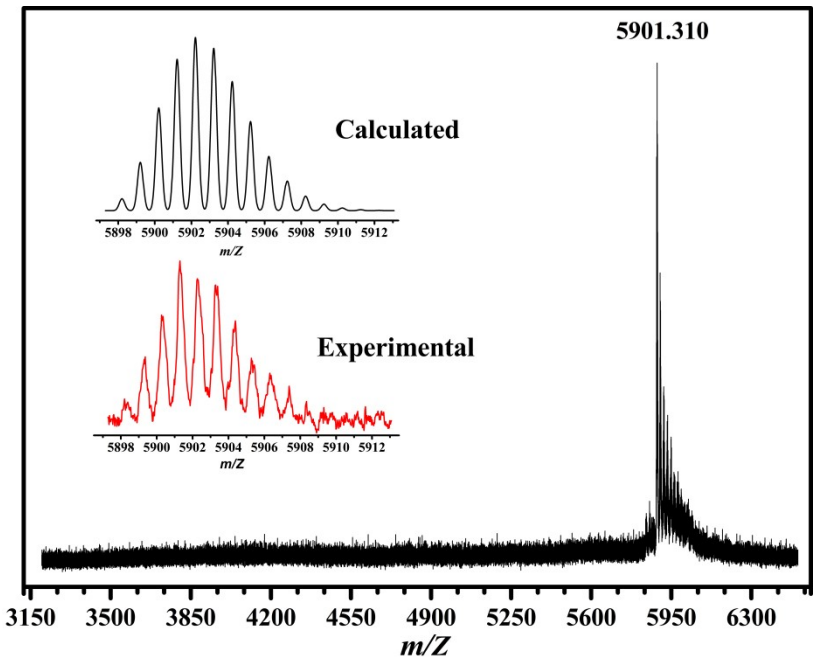

156

157 **Figure S3.** MALDI-TOF-MS mass spectrum of **CPOC-F301** from $CDCl_3$.

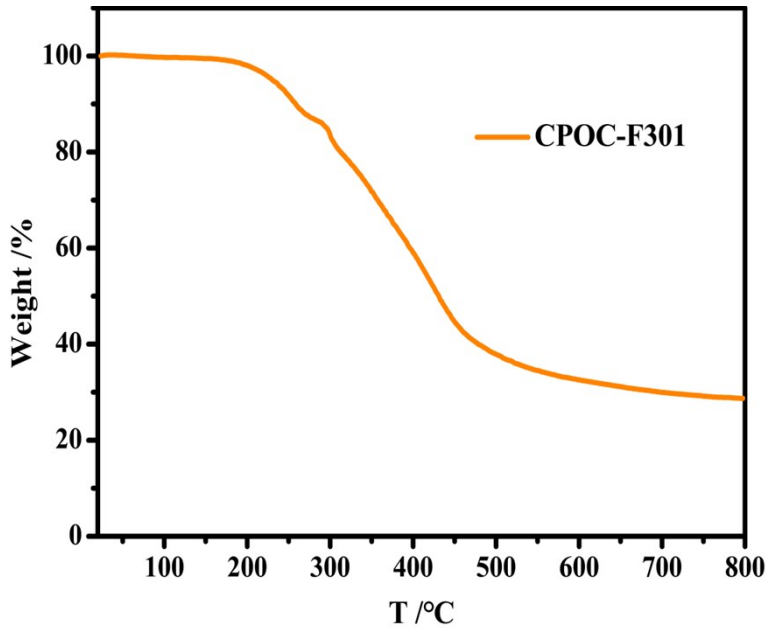

Figure S4. TGA curve of **CPOC-F301.**

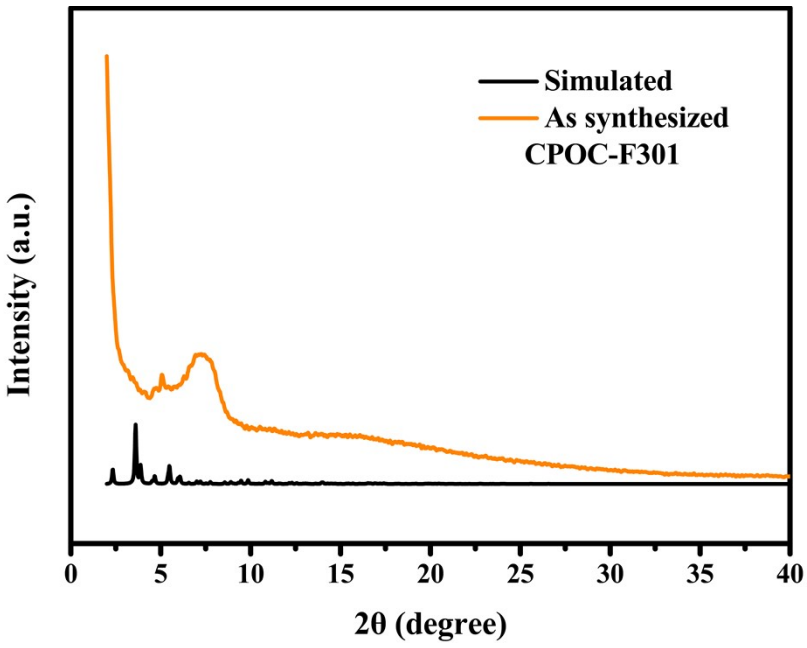

Figure S5. PXRD curves of **CPOC-F301**.

Note: the PXRD analysis showed that all the experimental powder X-ray diffractograms of **CPOC-F301** sample do not keep their original crystallinity compared to the powder X-ray diffractograms calculated from their single crystal structure data. This might be ascribed to that the packings of the isolated cage compounds are assembled by weak supramolecular interactions, which are different to MOFs and COFs assembled with much stronger coordination bonds and covalent bonds, respectively. These phenomena are often observed in cage system, especially for those with large cavities.[S5-7]

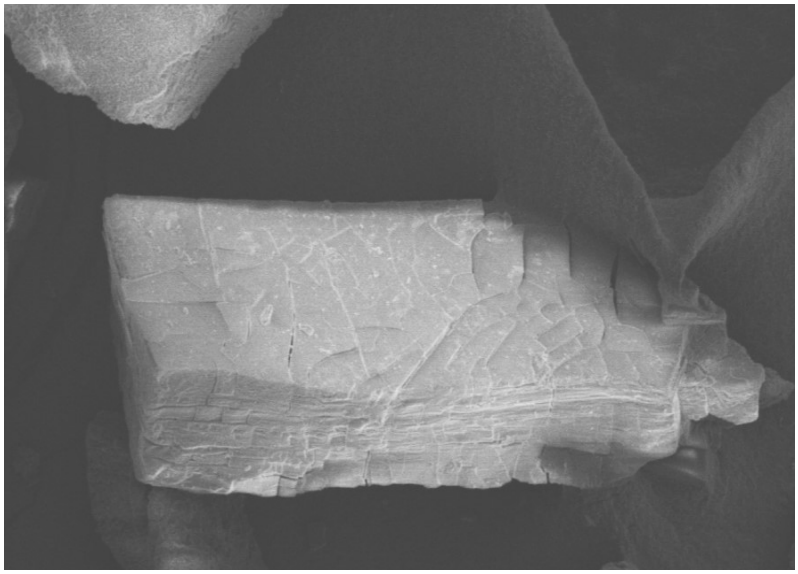

Figure S6. SEM image of **CPOC-F301.**

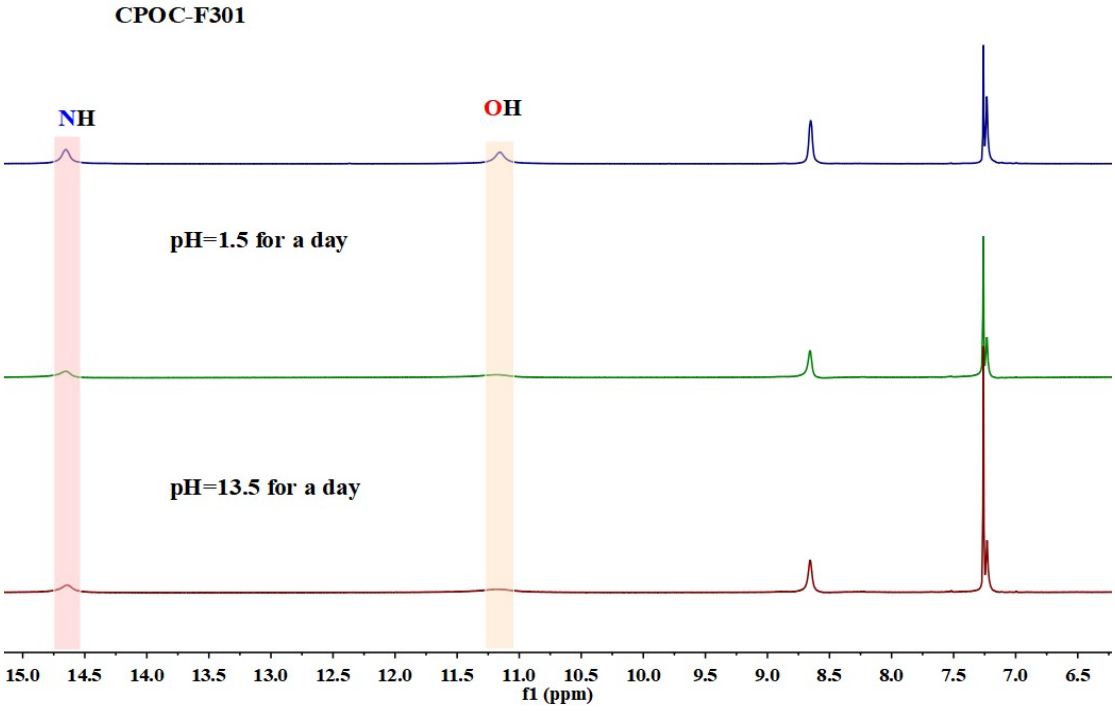

Figure S7. ^{1}H NMR spectra of **CPOC-F301** under various conditions.

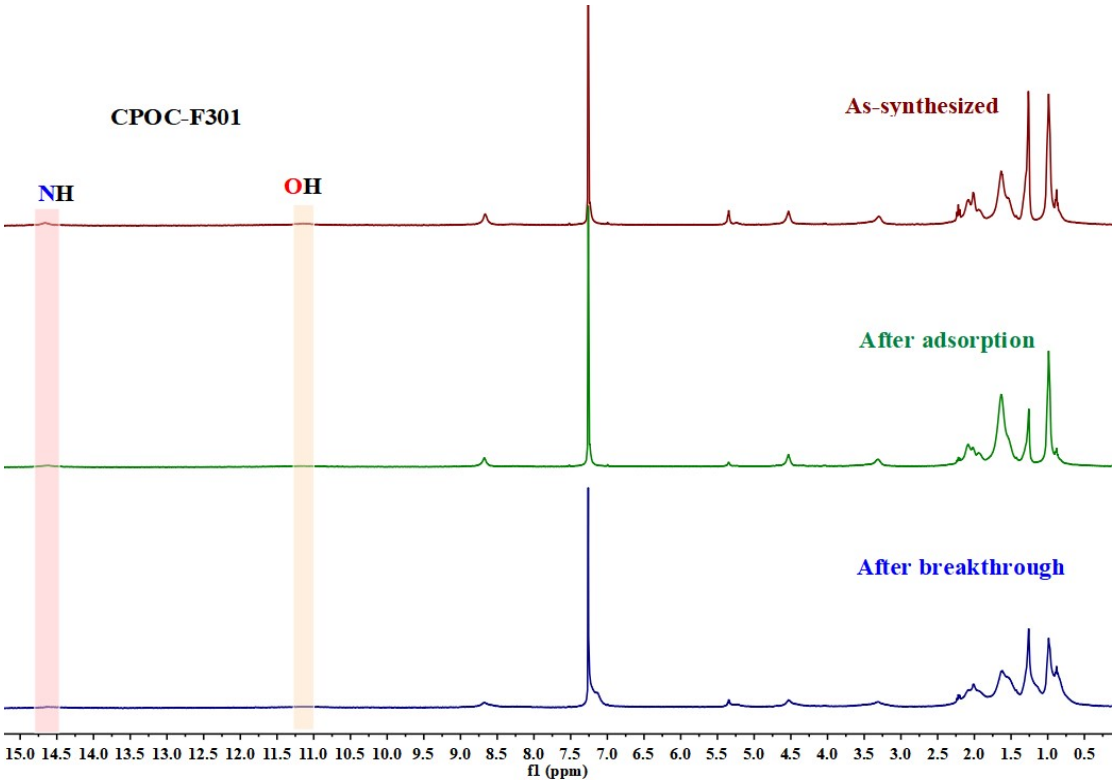

Figure S8. ^{1}H NMR spectra of **CPOC-F301** after adsorption and breakthrough tests.

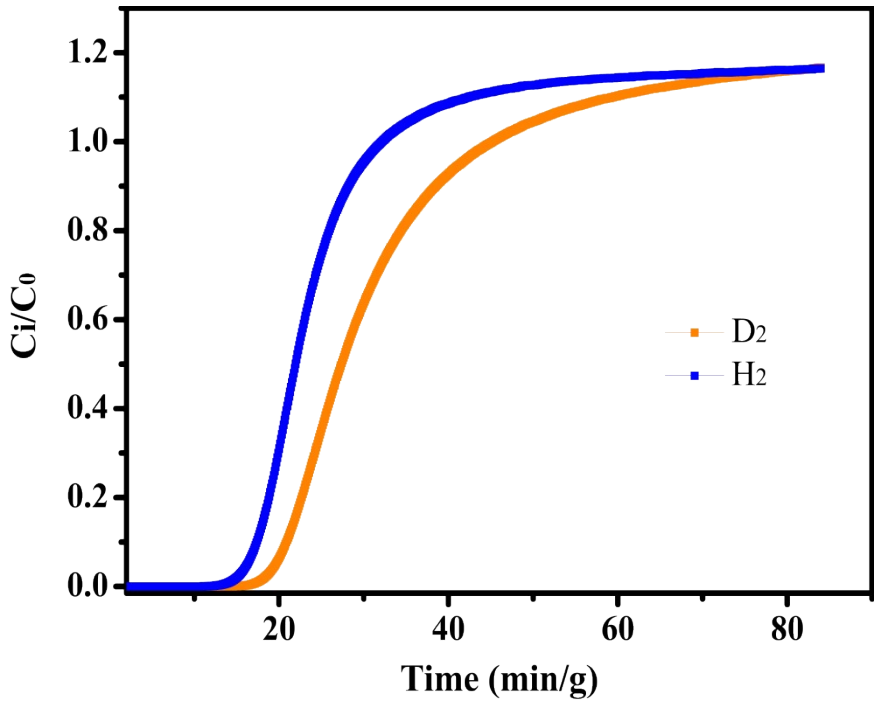

Figure S9. Dynamic breakthrough curves of **CPOC-F301** for D_2/H_2/Ne mixtures under 87 K, 3/3/94 (vol%), 8 mL/min.

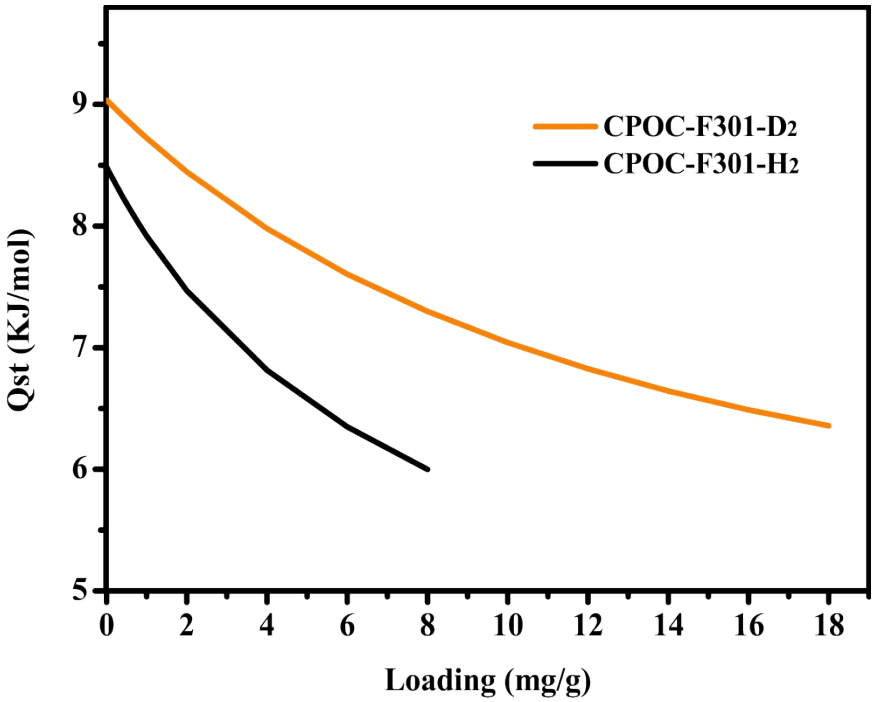

Figure S10. The isosteric heat of D_2 and H_2 for **CPOC-F301**.

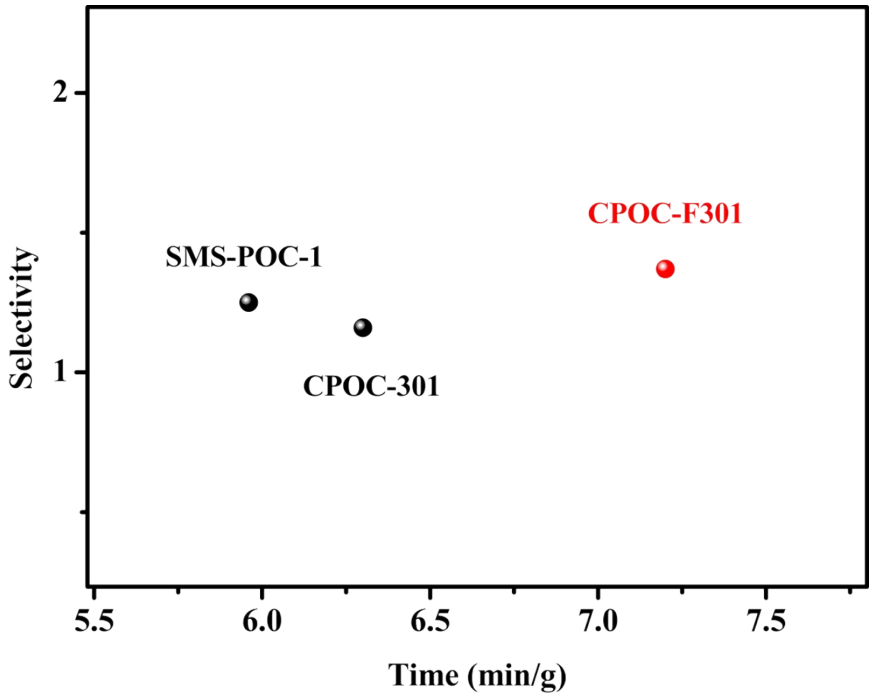

Figure S11. A comparison diagram of the separation data of the three crystals.

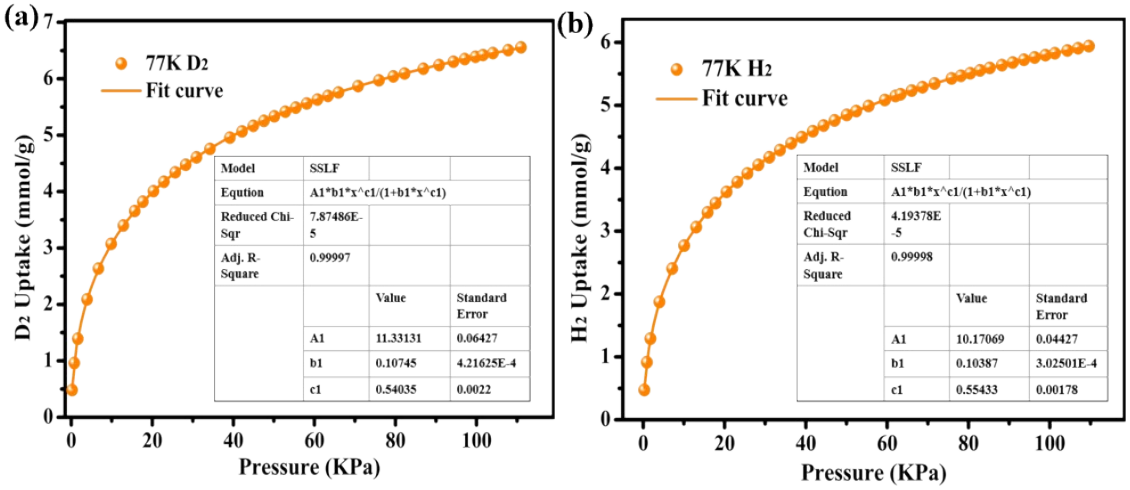

Figure S12. Single-site Langmuir-Freundlich fitting of (a) H_2 and (b) D_2 adsorption isotherm of **CPOC-F301** at 77 K.

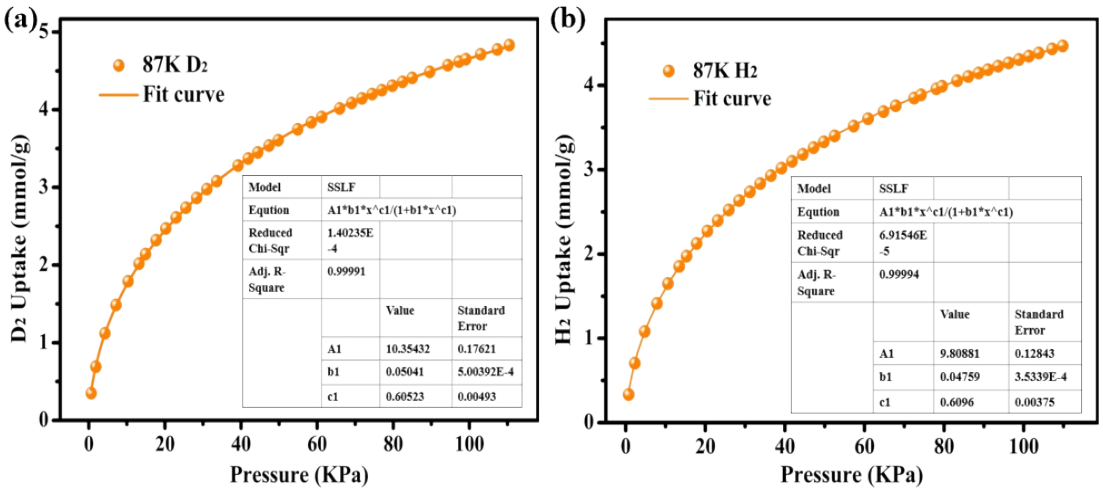

Figure S13. Single-site Langmuir-Freundlich fitting of (a) H_2 and (b) D_2 adsorption isotherm of **CPOC-F301** at 87 K.

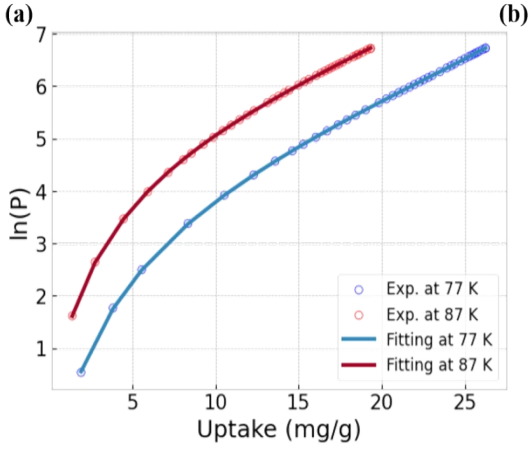

	Parameter Value	Standard Deviation
a_0	-1.087012e+03	4.747320e+00
a_1	4.005577e+01	9.606158e-01
a_2	-2.476989e+00	9.781192e-02
a_3	1.161779e-01	8.506738e-03
a_4	-3.305687e-03	3.265564e-04
a_5	3.876163e-05	4.590400e-06
b_0	1.335232e+01	5.668285e-02
b_1	-1.287245e-01	1.068636e-02
b_2	4.266252e-03	4.532988e-04
Adj.r_squared	0.9999	

Figure S14. (a) Virial equation fitting of D_2 adsorption isotherm of **CPOC-F301** at

77 K and 87 K. (b) Relevant fitting parameters for D_2.

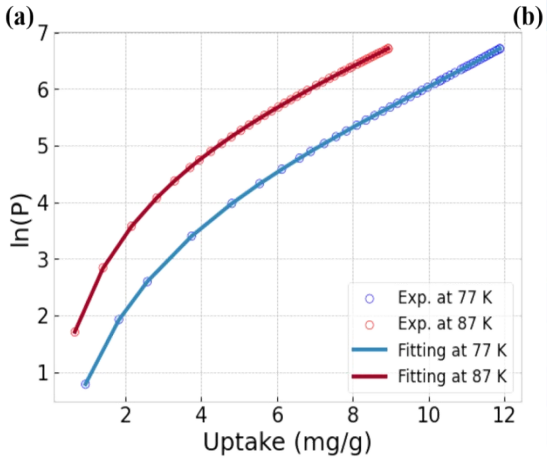

	Parameter Value	Standard Deviation
a_0	-1.020848e+03	2.441086e+00
a_1	7.727080e+01	1.059891e+00
a_2	-9.783091e+00	2.414917e-01
a_3	9.668802e-01	4.566426e-02
a_4	-5.751852e-02	3.830684e-03
a_5	1.459888e-03	1.179912e-04
b_0	1.343978e+01	2.906208e-02
b_1	-2.136464e-01	1.159024e-02
b_2	1.378394e-02	1.046501e-03
Adj.r_squared	0.9999	

Figure S15. (a) Virial equation fitting of H_2 adsorption isotherm of **CPOC-F301** at 77 K and 87 K. (b) Relevant fitting parameters for H_2.

Table S2. Summary table of hydrogen isotope separation performance for different porous materials at 1 bar and 77 K.

Compound	D_2 (cm^3/g)	H_2 (cm3/g)	Qst-D_2 (KJ/mol)	Qst-H_2 (KJ/mol)	Selectivity	Time (min/g)	Ref.
CPOC-F301	147	134	9.03	8.48	1.37	7.2	This work
CPOC-301	159	145	8.29	8.17	1.25	5.96	
SMS-POC-1	163	151	7.67	7.40	1.16	6.3	
FJI-Y11	205	183	7.88	7.13	1.76	17	S8
Zn-MOF-74	212.8	190.4	9.2	8.3	1.75	0	S9
Mg-MOF-74	296	271	12.8	11.3	3.24	10	
Ni-MOF-74	106	74	13.7	12.1	1.44	17	
Cu-BTB	138	121	10.9	10.5	1.87	6.2	S10
ECUT-8	208	186	8.4	7.9	1.38	4	S11
FJI-Y9	221.9	202.3	6.2	6.0	1.3	--	S12
FIR-29	149.7	136.8	6.1	5.8	1.2	--	

Cu-BTT	288	266	10.5	9.5	1.76	16	S13
MIL-101(Cr)	270	240	12.5	12	1.4	28	S14
ZJNU-119	358	325	7.6	7.2	1.37	38	S15
c-1a′	88.8	80.6	≈8.8	≈8.8	1.6	7.5	S16
Activated 2	301	278	7.45	6.85	1.53	52	S17

209 --means the information was not given.

210

211

212

Section S4. Various characterization data of the control group materials

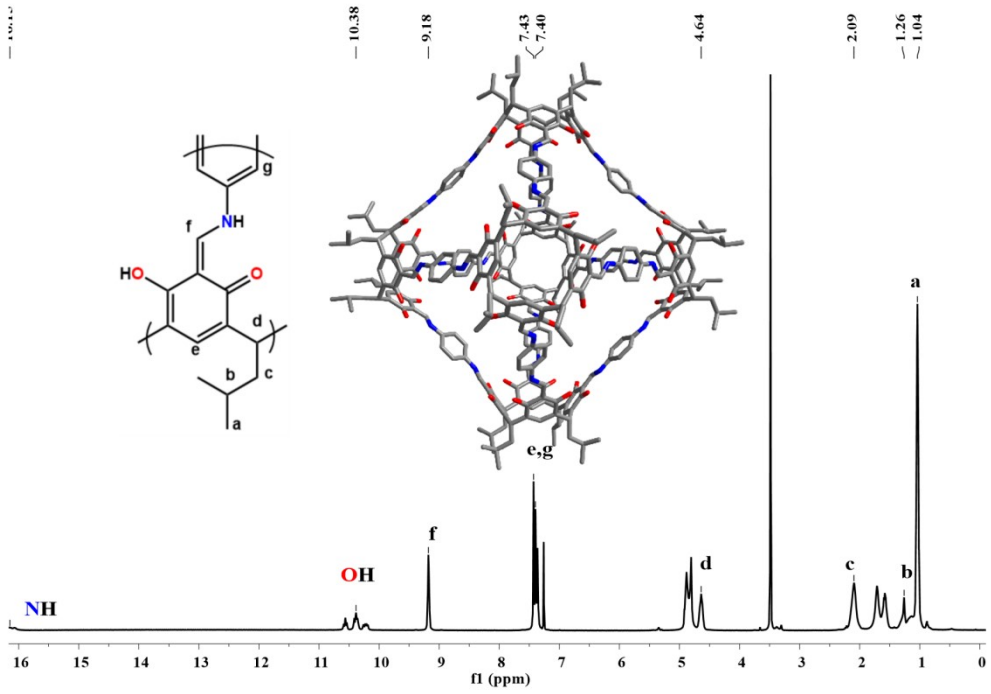

Figure S16. ^{1}H NMR spectrum of **CPOC-301**.

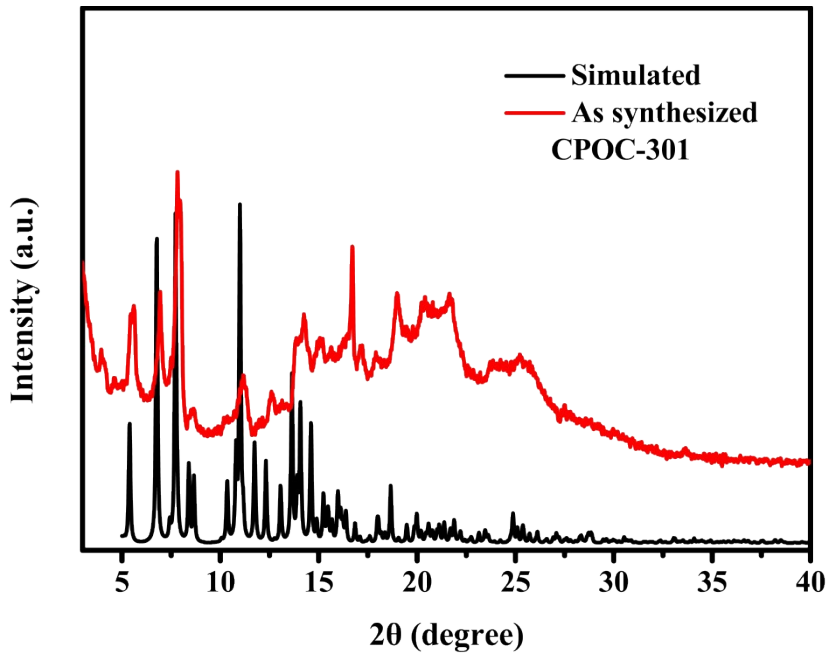

Figure S17. PXRD curves of **CPOC-301**.

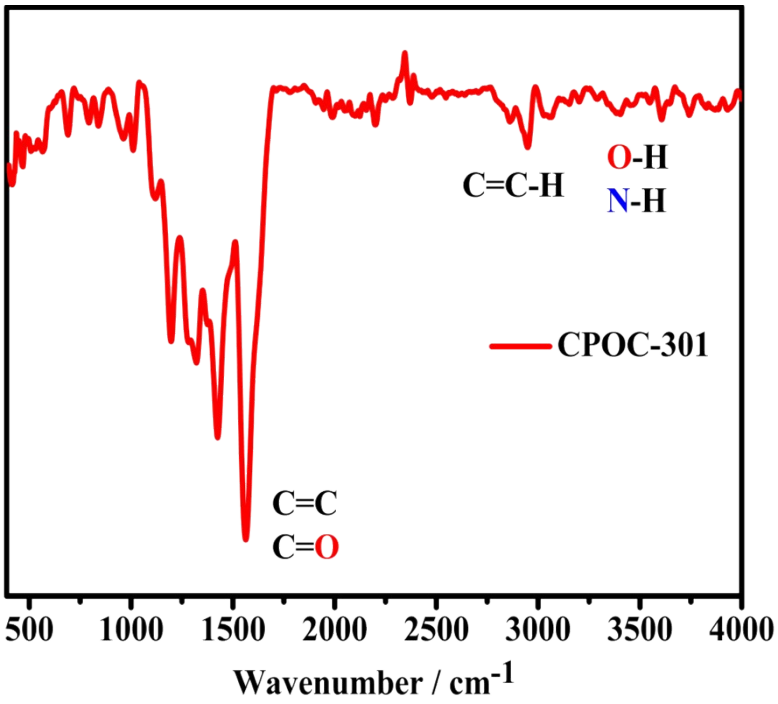

Figure S18. FT-IR spectrum of **CPOC-301**.

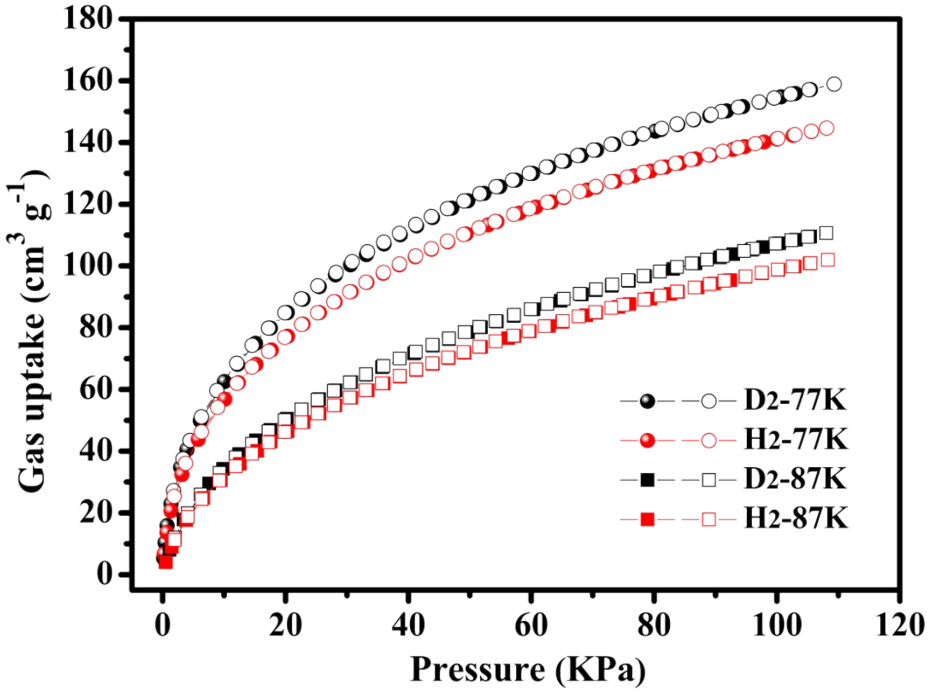

Figure S19. The adsorption isotherms of **CPOC-301** at temperatures of 77 K and 87 K.

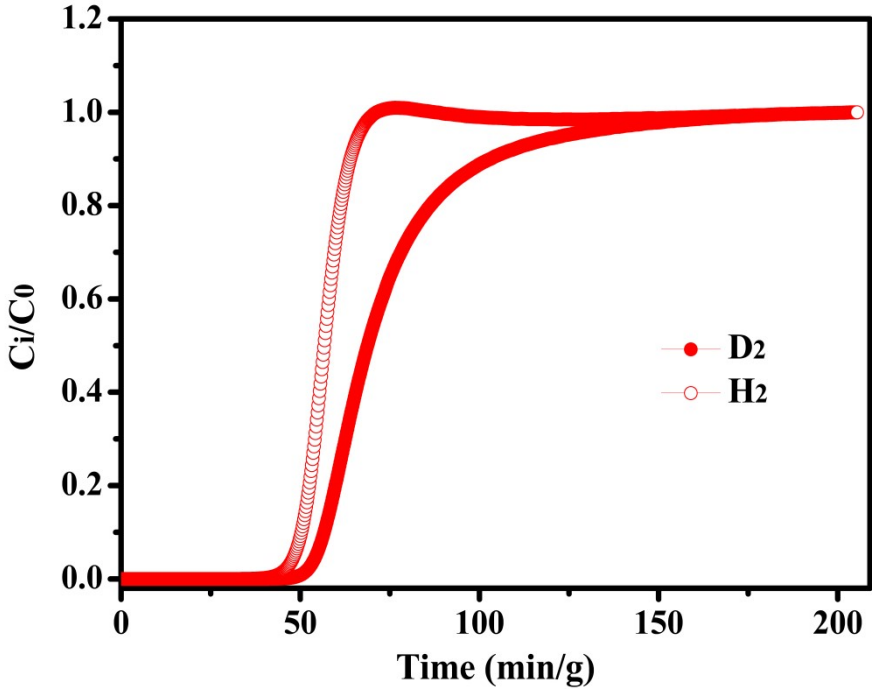

Figure S20. Experimental breakthrough curves of **CPOC-301** for the mixed gases of $D_2/H_2/Ne$ (3/3/94, v/v) at 77 K and 1 bar.

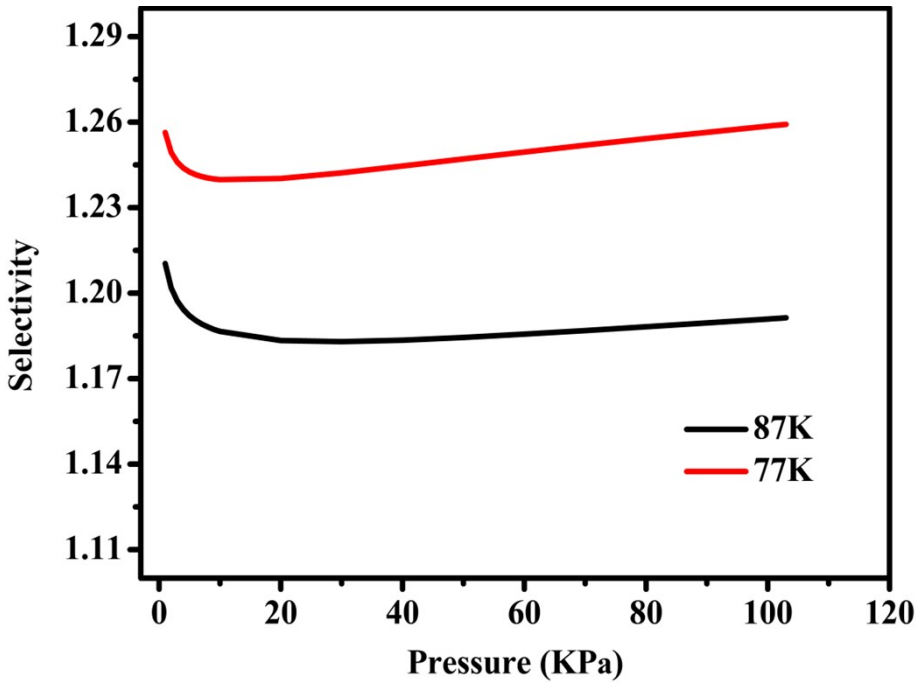

Figure S21. IAST selectivity of **CPOC-301** for equimolar D_2/H_2 mixture at 77 K and 87 K.

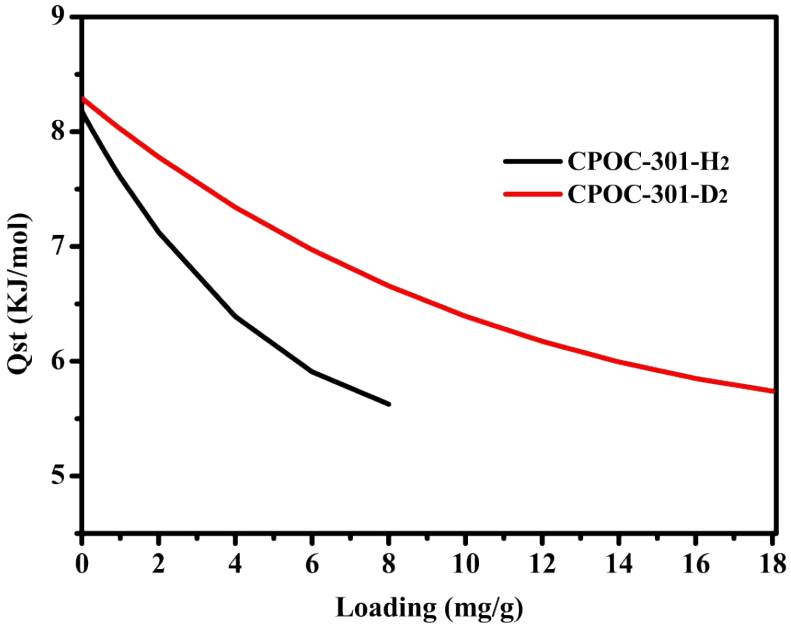

Figure S22. Qst values of D_2 and H_2 for **CPOC-301**.

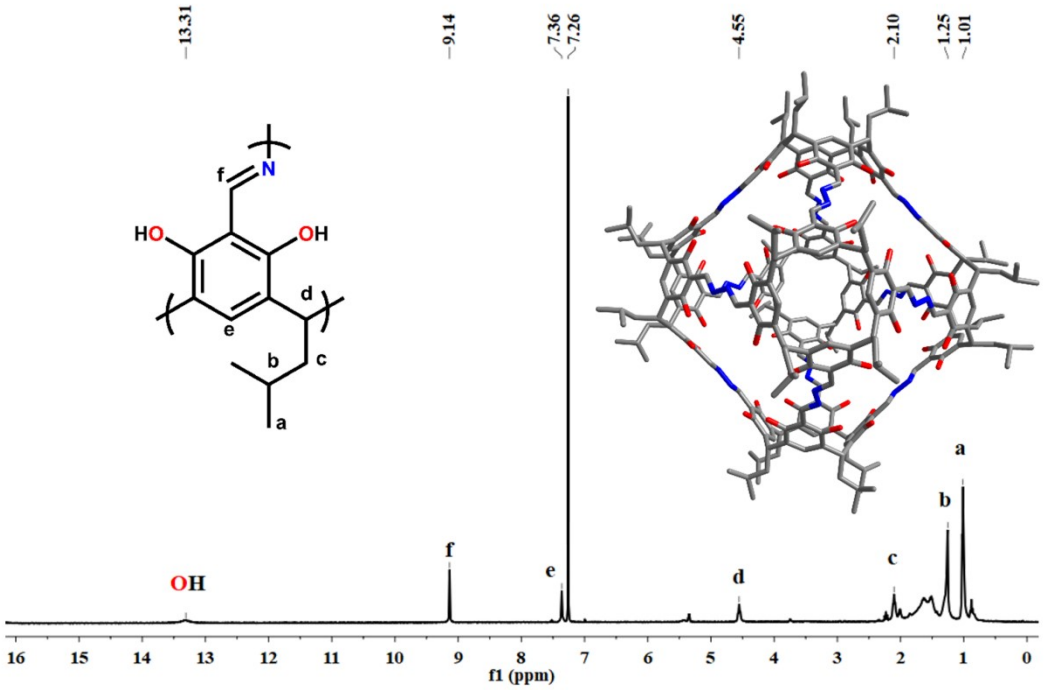

Figure S23. ^1H NMR spectrum of **SMS-POC-1**.

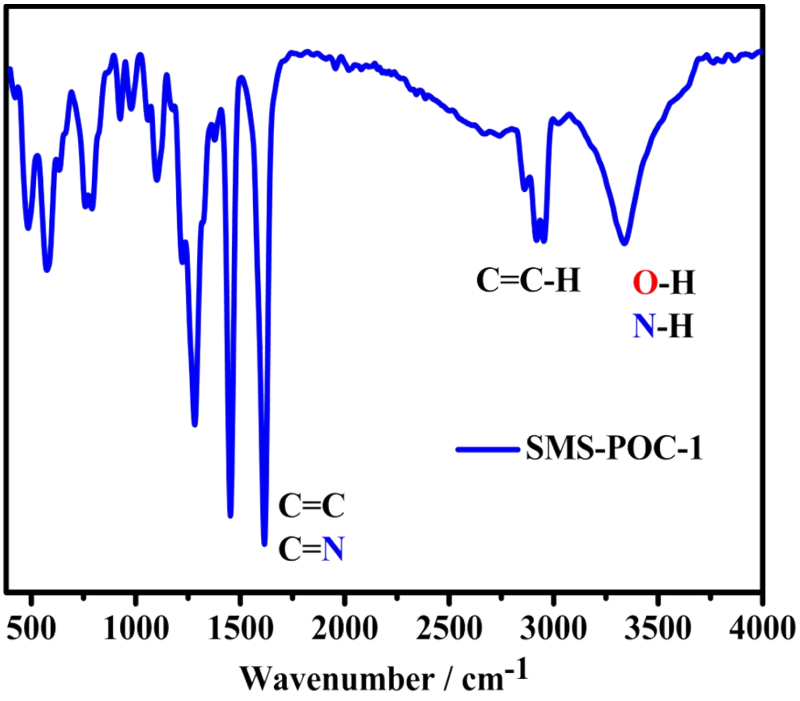

238

239 **Figure S24.** FT-IR spectrum of **SMS-POC-1**.

240

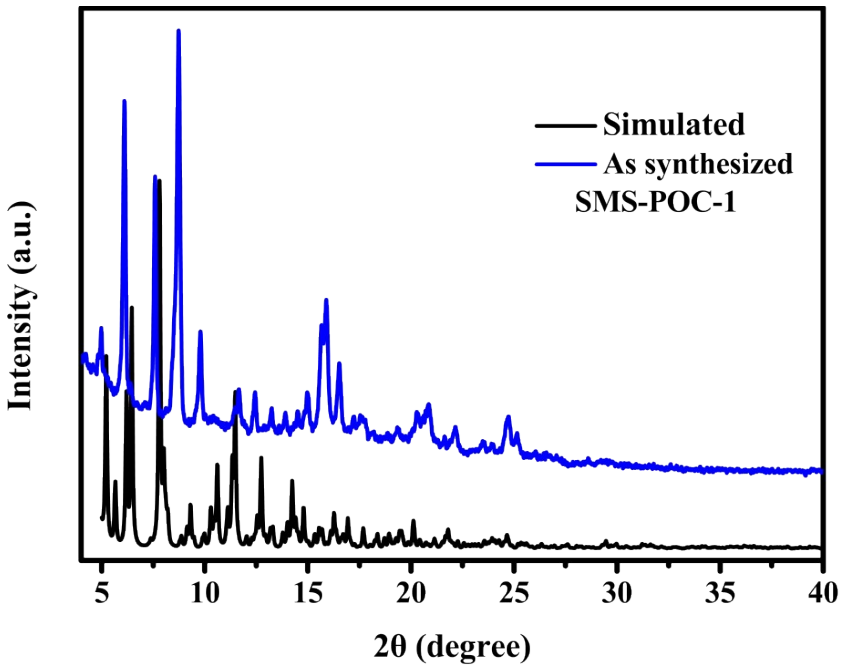

241

242 **Figure S25.** PXRD curves of **SMS-POC-1**.

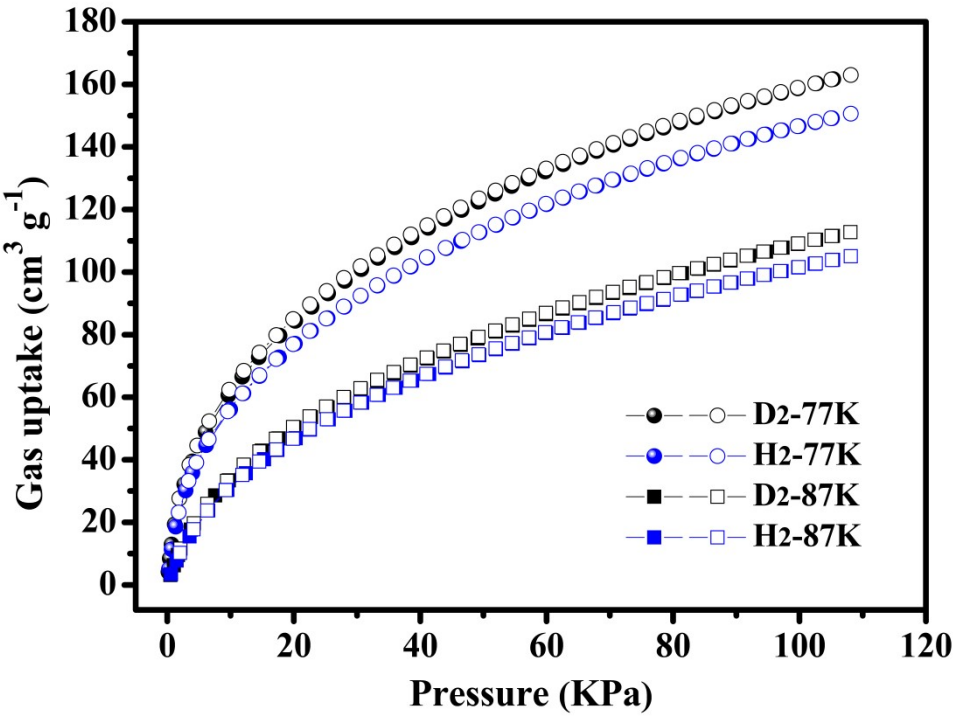

Figure S26. The adsorption isotherms of **SMS-POC-1** at temperatures of 77 K and 87 K.

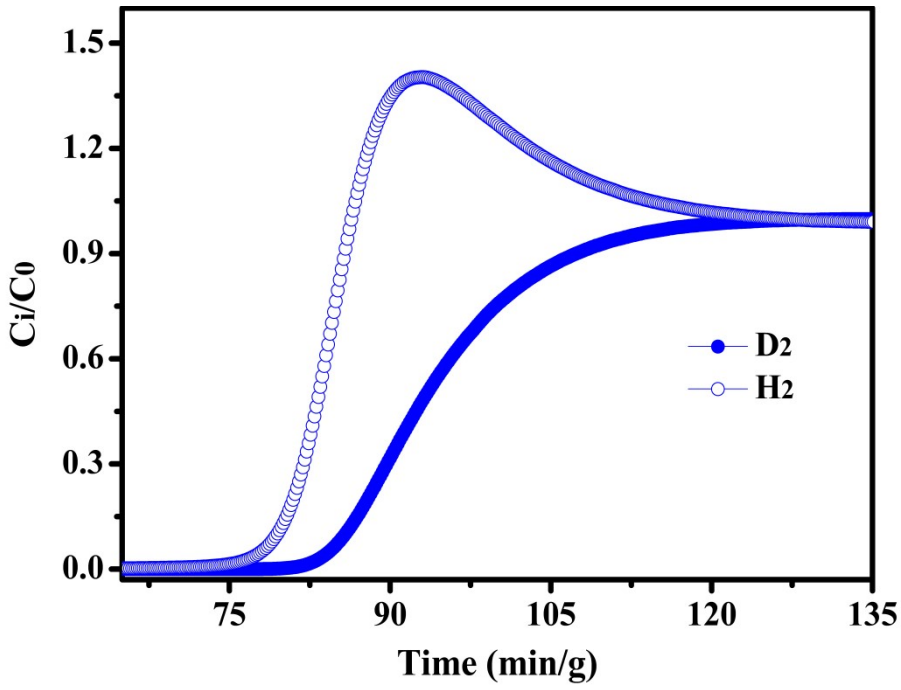

Figure S27. Experimental breakthrough curves of **SMS-POC-1** for the mixed gases of D_2/H_2/Ne (3/3/94, v/v) at 77 K and 1 bar.

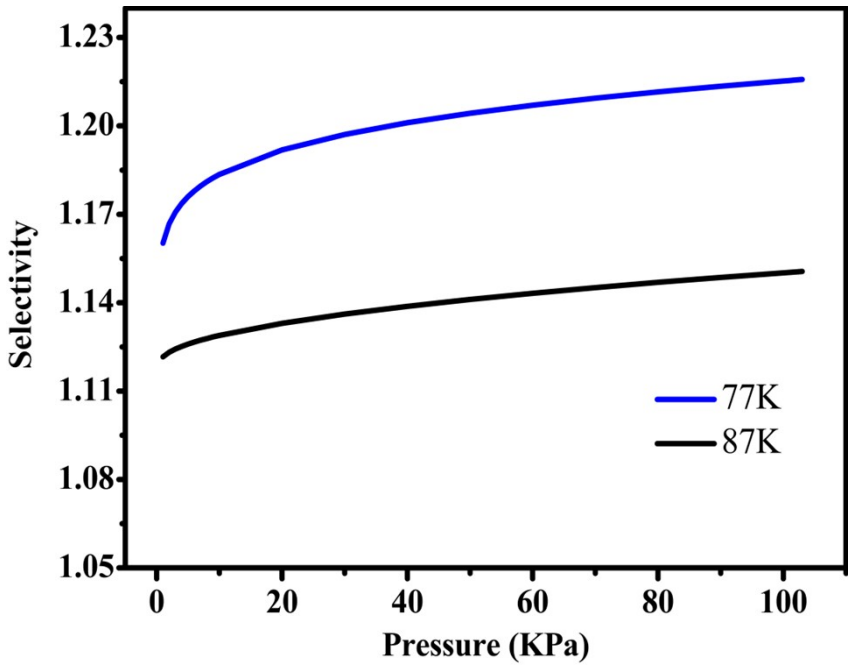

Figure S28. IAST selectivity of **SMS-POC-1** for equimolar D_2/H_2 mixture at 77 K and 87 K.

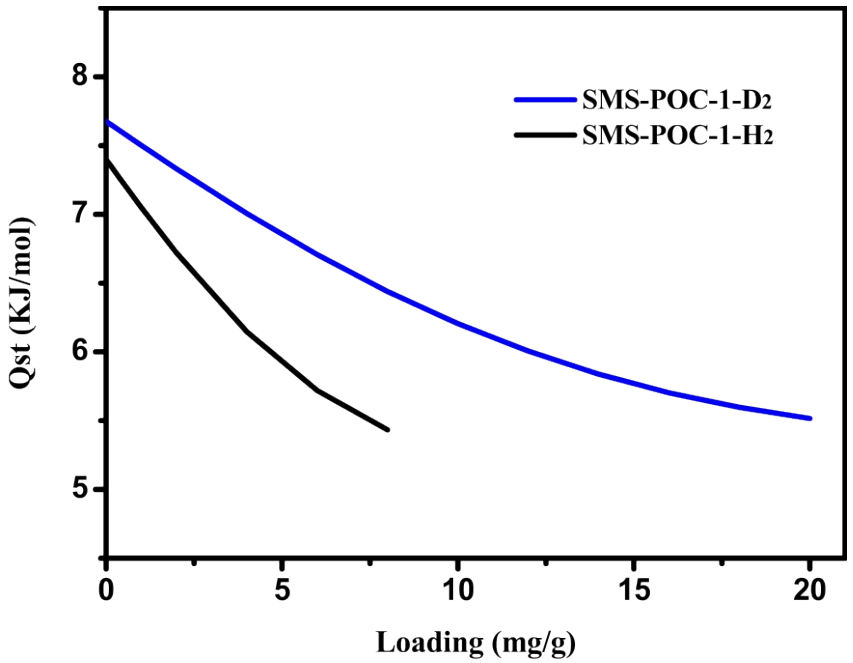

Figure S29. Qst values of D_2 and H_2 for **SMS-POC-1**.

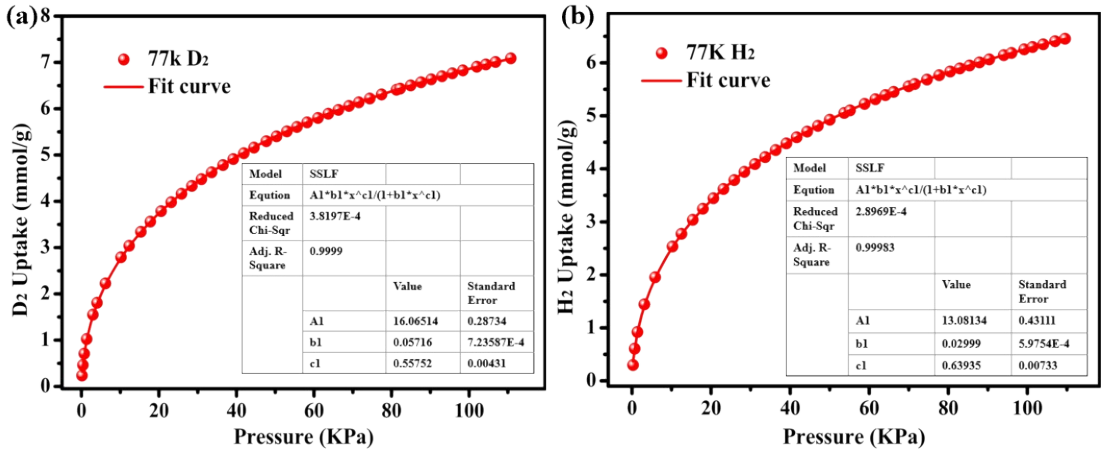

Figure S30. Single-site Langmuir-Freundlich fitting of (a) H_2 and (b) D_2 adsorption isotherm of **CPOC-301** at 77 K.

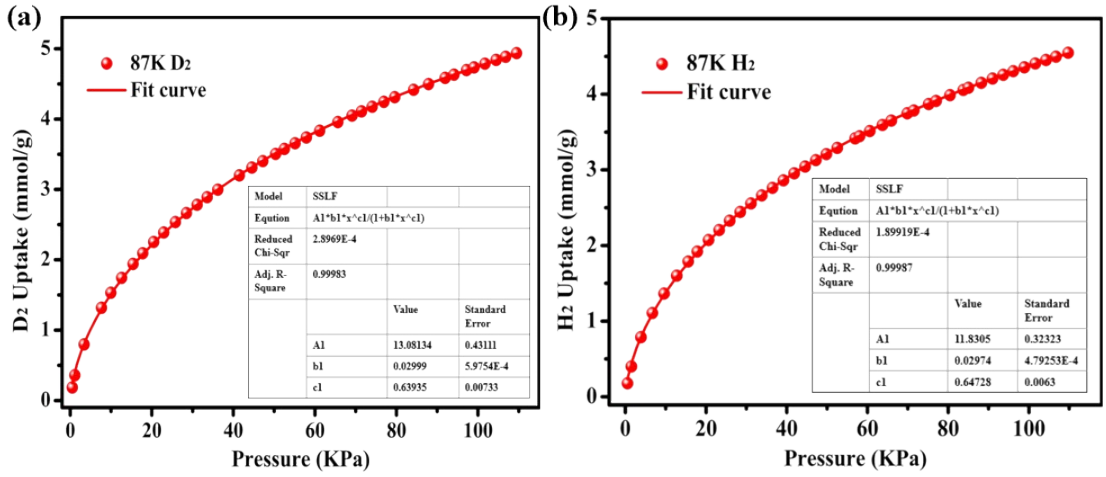

Figure S31. Single-site Langmuir-Freundlich fitting of (a) H_2 and (b) D_2 adsorption isotherm of **CPOC-301** at 87 K.

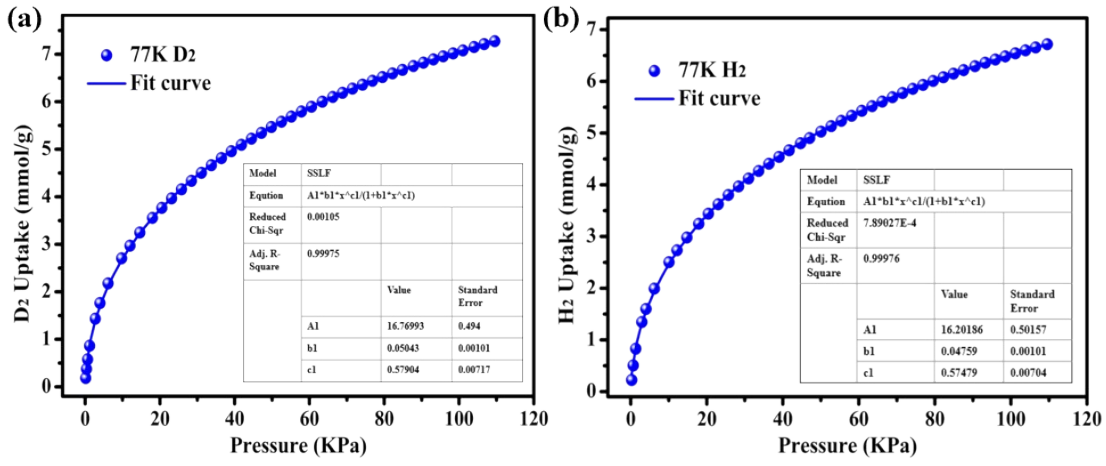

Figure S32. Single-site Langmuir-Freundlich fitting of (a) H_2 and (b) D_2 adsorption isotherm of **SMS-POC-1** at 77 K.

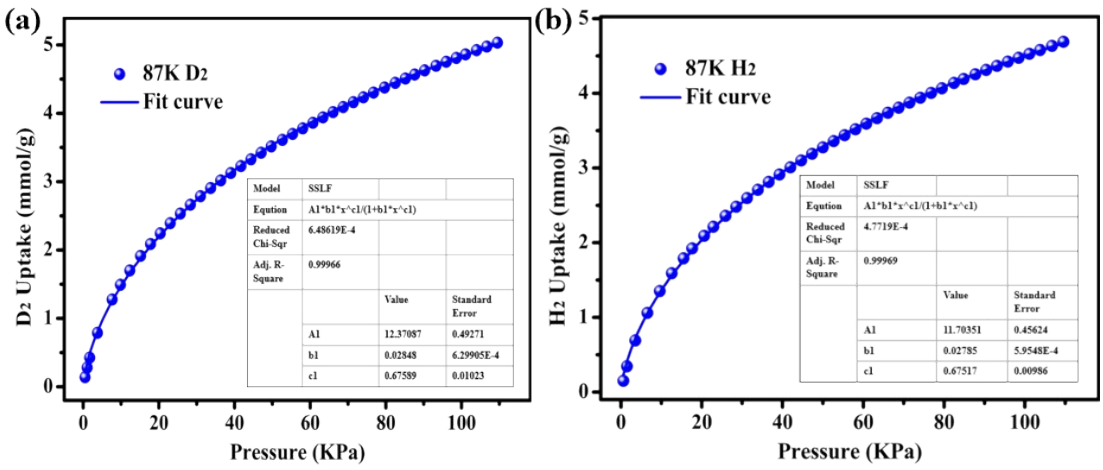

Figure S33. Single-site Langmuir-Freundlich fitting of (a) H_2 and (b) D_2 adsorption isotherm of **SMS-POC-1** at 87 K.

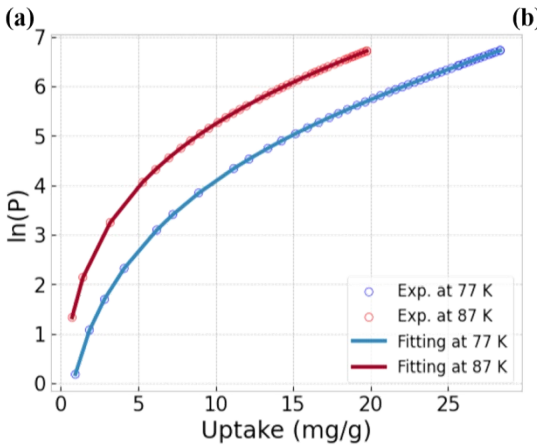

(b)

	Parameter Value	Standard Deviation
a_0	-9.973845e+02	1.323017e+00
a_1	3.333993e+01	2.674757e-01
a_2	-1.307655e+00	2.261242e-02
a_3	3.091069e-02	1.901545e-03
a_4	-5.533347e-04	7.071623e-05
a_5	4.439662e-06	9.515847e-07
b_0	1.294203e+01	1.611287e-02
b_1	-1.650573e-01	3.153902e-03
b_2	4.829095e-03	1.362054e-04
Adj.r_squared	0.9999	

Figure S34. (a) Virial equation fitting of D_2 adsorption isotherm of **CPOC-301** at 77 K and 87 K. (b) Relevant fitting parameters for D_2.

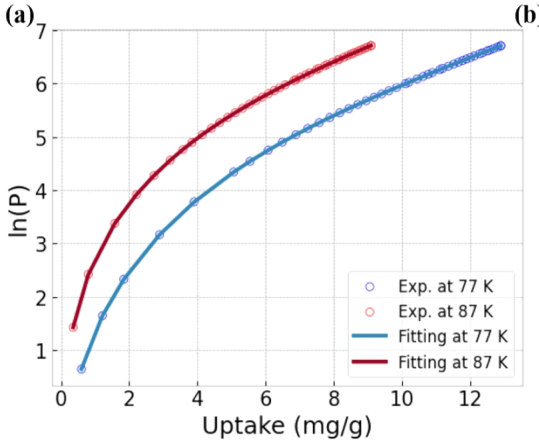

(b)

	Parameter Value	Standard Deviation
a_0	-9.834776e+02	1.123007e+00
a_1	7.461373e+01	4.856495e-01
a_2	-6.111605e+00	8.904298e-02
a_3	2.482054e-01	1.598417e-02
a_4	-6.832363e-03	1.293794e-03
a_5	5.779765e-05	3.801909e-05
b_0	1.360743e+01	1.349275e-02
b_1	-4.043218e-01	5.583233e-03
b_2	2.710404e-02	5.175743e-04
Adj.r_squared	0.9999	

Figure S35. (a) Virial equation fitting of H_2 adsorption isotherm of **CPOC-301** at 77 K and 87 K. (b) Relevant fitting parameters for H_2.

(a)

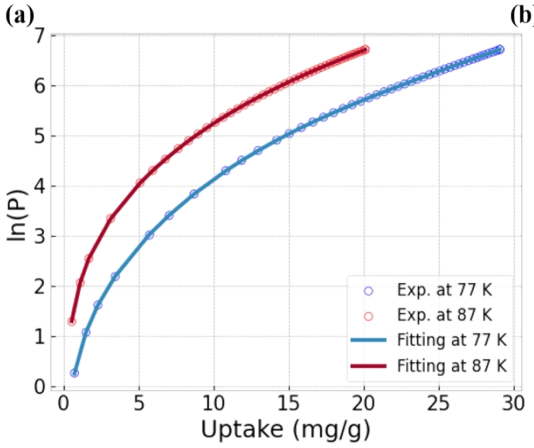

(b)

	Parameter Value	Standard Deviation
a_0	-9.233254e+02	1.714840e+00
a_1	2.111285e+01	3.490952e-01
a_2	-1.400314e-01	2.869763e-02
a_3	-2.937260e-02	2.387799e-03
a_4	1.037068e-03	8.749046e-05
a_5	-1.164841e-05	1.156575e-06
b_0	1.243278e+01	2.084812e-02
b_1	-1.289874e-01	4.144229e-03
b_2	3.675403e-03	1.800111e-04
Adj.r_squared	0.9999	

Figure S36. (a) Virial equation fitting of D_2 adsorption isotherm of **SMS-POC-1** at 77 K and 87 K. (b) Relevant fitting parameters for D_2.

(a)

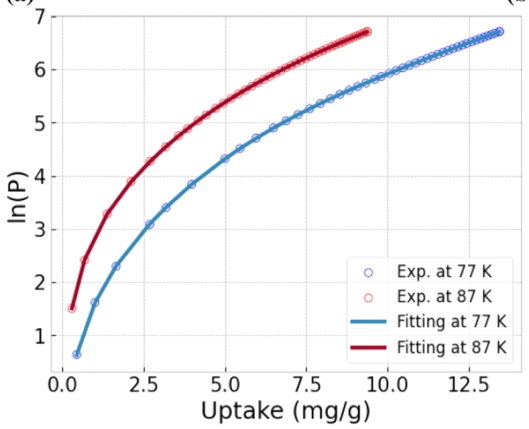

(b)

	Parameter Value	Standard Deviation
a_0	-8.900637e+02	1.728725e+00
a_1	4.256653e+01	7.195416e-01
a_2	-2.918477e-01	1.253889e-01
a_3	-3.177794e-01	2.223848e-02
a_4	2.339368e-02	1.749871e-03
a_5	-5.626446e-04	4.981455e-05
b_0	1.286194e+01	2.094567e-02
b_1	-2.635895e-01	8.491157e-03
b_2	1.615251e-02	7.698583e-04
Adj.r_squared	0.9999	

Figure S37. (a) Virial equation fitting of H_2 adsorption isotherm of **SMS-POC-1** at 77 K and 87 K. (b) Relevant fitting parameters for H_2.

Section S5. References

S1. M. Grajda, M. Wierzbicki, P. Cmoch and A. Szumna, *J. Org. Chem.*, 2013, **78**, 11597-11601.

S2. G. M. Sheldrick, *Acta Crystallogr. C.*, 2015, **71**, 3-8.

S3. K. E. Jelfs, X. Wu, M. Schmidtmann, J. T. A. Jones, J. E. Warren, D. J. Adams and A. I. Cooper, *Angew. Chem. Int. Ed.*, 2011, **50**, 10653-10656.

S4. B. Teng, M. A. Little, T. Hasell, S. Y. Chong, K. E. Jelfs, R. Clowes, M. E. Briggs and A. I. Cooper, *Cryst. Growth Des.*, 2019, **19**, 3647-3651.

S5. P. Wagner, F. Rominger, W.-S. Zhang, J. H. Gross, S. M. Elbert, R. R. Schroeder and M. Mastalerz, *Angew. Chem. Int. Ed.*, 2021, **60**, 8896-8904.

S6. D. Beaudoin, F. Rominger and M. Mastalerz, *Angew. Chem. Int. Ed.*, 2017, **56**, 1244-1248.

S7. S. Hong, M. R. Rohman, J. Jia, Y. Kim, D. Moon, Y. Kim, Y. H. Ko, E. Lee and K. Kim, *Angew. Chem. Int. Ed.*, 2015, **54**, 13241-13244.

S8. Y. A. Si, X. He, J. Jiang, Z. M. Duan, W. J. Wang and D. Q. Yuan, *Nano Res.*, 2021, **14**, 518-525.

S9. Y. N. Si, W. J. Wang, E. M. El-Sayed and D. Q. Yuan, *Sci. China Chem.*, 2020, **63**, 881-889.

S10. X. F. Li, Z. F. Ju, K. Z. Su, W. J. Wang and D. Q. Yuan, *Mater. Chem. Front.*, 2025, **9**, 2508-2513.

S11. M. Yin, R. Krishna, W. Wang, D. Yuan, Y. Fan, X. Feng, L. Wang and F. Luo, *CCS Chem.*, 2022, **4**, 1016-1027.

S12. F.-J. Zhao, Y.-X. Tan, W. Wang, Z. Ju and D. Yuan, *Inorg. Chem.*, 2018, **57**, 13312-13317.

S13. Y. P. Huang, Z. F. Ju, K. Z. Su, W. J. Wang and D. Q. Yuan, *Inorg. Chem.*, 2025, **64**, 1203-1207.

S14. L. Yuan, X. T. Huang, J. Y. Zhu, K. Z. Su, W. J. Wang and D. Q. Yuan, *Inorg. Chem.*, 2025, **64**, 10238-10242.

S15. Y. Guo, K. Su, W. Wang and D. Yuan, *Inorg. Chem.*, 2025, **64**, 18599-18603.

S16. W. Zhou, Y. Li, L. Xiong, W. Wang, R. Guan, Z. Chen, D. Yuan, E.-Q. Gao and D. Zhang, *J. Am. Chem. Soc.*, 2025, **147**, 35664-35674.

S17. Z. Xie, Z. Zhuo, Z. A. Nan, Q. Li, W. Wu, Y. Zhou, Z. X. Lu, J. Liu, L. Liu, W. Wang, D. Yuan and Y. G. Huang, *Adv. Sci.*, 2025, DOI: 10.1002/advs.202519498.